Journal of Nano- and Electronic Physics
Vol. **8** No 4, 04003(9pp) (2026)

Журнал нано- та електронної фізики
Том **18** № 4, 04003(9cc) (2026)

OPEN ACCESS

REGULAR ARTICLE

Microwave Behavior of PVC/YIG/Carbon Material Composite Films in X-band

L.M. Grishchenko[1,2], D.O. Zhytnyk[3], V.Yu. Malyshev[3], V.E. Diyuk[2,3], T.O. Plutenko[4], M.O. Popov[3], H.L. Chumak[3], I.P. Matushko[3,*], Yu.V. Noskov[5], V.V. Kyrychenko[3], M.V. Makarets[3], V.V. Lisnyak[1,6]

[1] *Chuiko Institute of Surface Chemistry, National Academy of Science of Ukraine, 03164 Kyiv, Ukraine*
[2] *Institute of Engineering Thermophysics, National Academy of Science of Ukraine, 03057 Kyiv, Ukraine*
[3] *Taras Shevchenko National University of Kyiv, 01601 Kyiv, Ukraine*
[4] *V.I. Vernadsky Institute of General and Inorganic Chemistry, National Academy of Science of Ukraine, 03142 Kyiv, Ukraine*
[5] *Kukhar Institute of Bioorganic Chemistry and Petrochemistry, National Academy of Science of Ukraine, 02160 Kyiv, Ukraine*
[6] *Institute of Macromolecular Chemistry, National Academy of Science of Ukraine, 02155 Kyiv, Ukraine*

(Received 05 May 2026; revised manuscript received 19 August 2026; published online 21 August 2026)

This study reports the fabrication and microwave characterization of flexible poly(vinyl chloride) (PVC)–based composite films containing yttrium–iron garnet (YIG) and carbon fillers with different morphology, namely multi-walled carbon nanotubes (MWCNTs), carbon nanoparticles (CNPs), and activated carbon (AC). Composite films with a thickness of approximately 0.25 mm were prepared by hot pressing at 175 °C and 10 MPa, using 20 wt.% YIG, 10 wt.% carbon filler (relative to PVC), and dibutyl phthalate as a plasticizer. The used fillers were characterized by scanning electron microscopy (SEM), and thermogravimetric analysis. SEM analysis revealed that the YIG powder consists of agglomerated, nearly spherical crystallites. The IR spectra of the composite films demonstrated characteristic absorption bands of PVC and YIG; when introducing fillers, slight shifts of individual characteristic bands of the polymer were observed, which indicates a slight interaction between the fillers and the PVC matrix. X-band (8–12 GHz) microwave measurements demonstrated a strong dependence of reflection, transmission, and absorption on the nature of the carbon filler. Compared to neat PVC, electromagnetic wave absorption increased markedly following the trend MWCNTs > CNPs > AC across the entire frequency range. At 8 GHz, absorption increased from approximately 5.6% (AC) to 26.3% (CNPs); at 10 GHz, from 4.4% (AC) to 26.1% (MWCNTs); and at 12 GHz, from 4.9% (AC) to 31% (MWCNTs). The smallest enhancement in absorption was achieved for the PVC/YIG/AC composite, whereas the largest increase was achieved for the PVC/YIG/MWCNT films. These results demonstrate that carbon filler morphology plays a decisive role in governing the microwave absorption behavior of PVC/YIG/carbon composites. Among the investigated fillers, MWCNTs provide the most efficient microwave absorption in the X-band, highlighting the potential of these ternary composites for use in lightweight, flexible microwave-absorbing and electromagnetic irradiation-shielding coatings, which will provide protection from electromagnetic radiation.

Keywords: Yttrium iron garnet, Polyvinyl chloride, Composite material, Carbon materials, Electromagnetic shielding, Microwave absorbing materials.

DOI: 10.21272/jnep.18(4).04003 PACS numbers: 41.20.Jb, 77.22.Gm, 82.35.Np

1. INTRODUCTION

The unprecedented technological progress of the 21st century has significantly increased the use of electronic devices, thereby contributing to the growing problem of electromagnetic pollution. This phenomenon negatively affects both the environment and biological systems [1, 2]. Consequently, a wide range of approaches has been proposed to protect biological and technical objects from electromagnetic radiation generated by electromagnetic fields [3, 4]. In this context, the development of multifunctional microwave-absorbing materials with low density and small thickness has attracted considerable scientific and practical interest [5, 6]. Carbon-based materials have received significant attention in the field of microwave absorption owing to their natural abundance, low cost, environmental friendliness, good electrical conductivity, high specific surface area, ease of surface modification, and chemical stability [7-9]. Among them, carbon nanotubes (CNTs) [10], graphene [11], porous carbon [12], carbon black [13], biomass-derived carbon [14], and their hybrids [15] have emerged as key components for the fabrication of lightweight and efficient electromagnetic shielding and absorbing materials, due to their unique structures and stable physicochemical properties. The demand for electromagnetic wave absorbers continues to grow, as no single material

* mipigor@gmail.com

Cite this article as: L.M. Grishchenko et al., *J. Nano- Electron. Phys.* 18 No 4, 04003 (2026) https://doi.org/10.21272/jnep.18(4).04003

can simultaneously satisfy all performance requirements [16]. To improve microwave absorption efficiency, magnetic fillers, particularly ferrites, are often incorporated into carbon-containing composites. Ferrites have been intensively studied because of their low cost, environmental stability, high saturation magnetization, and pronounced magnetic losses [17-19]. The advantages of incorporating ferrite materials into radio-absorbing composites are well established [20]. First, magnetic fillers increase the effective magnetic permeability (μ_{eff}) of the composite, thereby reducing its reflection coefficient. Second, the introduction of magnetic components decreases the electrical thickness of the absorber, which is inversely proportional to $\sqrt{(\varepsilon\mu)}$, enabling comparable reflection characteristics to be achieved with thinner coatings. Finally, ferrite particles exhibit enhanced selective absorption of electromagnetic energy in frequency regions associated with magnetic moment precession. This absorption may occur either under an applied external magnetic field (induced ferromagnetic resonance) or in the absence of an external field (natural ferromagnetic resonance).

Yttrium-iron garnet (YIG, $Y_3Fe_5O_{12}$) is a ferrite material widely used in electronic and microwave devices. However, despite extensive research on binary polymer–carbon and polymer–ferrite systems, multicomponent polymer-based composites remain comparatively underexplored. In particular, the properties of ternary polymer–carbon–ferrite systems, as well as the influence of carbon filler morphology on the microwave response of thin-film composites, have not been systematically investigated.

In contrast to previous studies, the present work focuses on ternary poly(vinyl chloride) (PVC)–carbon–ferrite thin-film composites with a fixed ferrite loading and a controlled variation of carbon filler morphology, including carbon nanotubes, carbon nanoparticles, and activated carbon. By employing YIG as the magnetic component and comparing carbon fillers with fundamentally different dimensionality and electrical characteristics, this study establishes direct structure–property relationships between filler nature and microwave response in the X-band. Particular emphasis is placed on the simultaneous analysis of reflection, transmission, and absorption, enabling clear identification of carbon filler-dependent microwave loss mechanisms. To the best of our knowledge, such a comparative investigation of PVC-based ternary polymer–carbon and ferrite filled thin films and the explicit role of carbon morphology in tuning microwave properties has not been previously reported.

The aim of this work is to fabricate ternary polymer–carbon–ferrite composite systems based on PVC and to examine the microwave properties of their thin composite films.

2. DESCRIPTION OF OBJECTS AND INVESTIGATION METHODS

2.1 Reagents and Materials

Carbon fillers of different morphology used in this work are apricot pit–derived activated carbon carbon (AC), laboratory-produced carbon nanoparticles (CNPs), and multiwalled carbon nanotubes (MWCNTs) obtained from Sigma-Aldrich.

An industrial-grade YIG was used as the magnetic filler. Before composite fabrication, YIG powder was high-energy ball-milled in a Retsch PM 400 planetary mill using ZrO_2 jars and balls to reduce particle size and suppress agglomeration, ensuring improved dispersion in the polymer matrix. PVC with an average molecular weight $M_W \approx 80{,}000$–$120{,}000$ (K-value 67) and dibutyl phthalate (DBP), later used as a plasticizer, were also purchased from Sigma-Aldrich and used as received without further purification.

2.2 Fabrication of PVC/YIG/C Composites

For composite fabrication, we used the ball-milled YIG powder, while carbon fillers were lightly ground in an agate mortar to disintegrate loosely bound agglomerates without damaging their morphology. The PVC/YIG/carbon composite films were prepared by hot pressing of mechanically homogenized powder mixtures. In a typical procedure, predetermined amounts of YIG ferrite and carbon filler were first mixed and homogenized in an agate mortar. Subsequently, 0.14 g of PVC powder was introduced, and the resulting ternary mixture was thoroughly ground until a visually uniform dispersion was achieved. The homogenized powder blend was then transferred into a stainless-steel mold placed on a polyamide support, followed by the addition of 70 mg of DBP as a plasticizer. Hot pressing was carried out at 175 °C under a pressure of 10 MPa with a holding time of 1 min, yielding flexible composite films with uniform thickness. The investigated ternary PVC/YIG/C composition represents a typical three-component system containing 20 wt.% YIG and 10 wt.% carbon filler with respect to PVC. This formulation corresponded to the following component masses: PVC – 0.14 g, YIG – 0.04 g, carbon filler – 0.02 g, resulting in a total solid mass of 0.20 g prior to plasticizer addition.

2.3 Thermogravimetric Analysis (TGA)

Thermogravimetric and differential thermal gravimetric (TG/DTG) thermograms of dry samples were recorded at a heating rate of 10 °C min^{-1} under an argon flow of 100 mL min^{-1} using a McBain balance [21,22].

2.4 Scanning Electron Microscopy

Morphological studies were performed by scanning electron microscopy (SEM) using a Tescan Mira 3 LMU microscope operating in working distance (WD)–controlled mode [23]. The samples were mounted on aluminum stubs using conductive carbon tape. To minimize charging effects, non-conductive specimens were sputter-coated with a thin conductive layer. SEM imaging was carried out under high-vacuum conditions at accelerating voltages of 10 kV, with the working distance optimized (typically 8–12 mm) to achieve a balance between spatial resolution, depth of field, and signal intensity.

2.5 Energy-Dispersive X-ray Spectroscopy

Elemental composition were analyzed by energy-dispersive X-ray spectroscopy (EDX) using an Advanced

Aztec Energy (IE350) system equipped with an X-Max 80 silicon drift detector, integrated into the SEM. EDX spectra were acquired at an accelerating voltage of 15–20 kV in a WD-optimized acquisition geometry to ensure efficient X-ray collection. Quantitative analysis was performed using standardless ZAF correction, with results averaged over multiple regions to ensure representative compositional data.

2.6 Optical Microscopy

Optical images of the PVC/YIG/carbon composite films were acquired using a Bresser Analyth STR trinocular stereo optical microscope equipped with a MikroCamII 12 MP digital camera. The measurements were performed in reflected-light mode at magnifications of 10×–40×, which is suitable for imaging opaque composite films.

2.7 Microwave Measurements

The high-frequency microwave reflection (S_{11}) and transmission (S_{21}) losses of the prepared composite materials were measured using a scalar network analyzer operating in the X-band (8–12 GHz) and a standard metallic rectangular waveguide configuration [23-25]. The measurements were performed in a two-port geometry, where the sample under investigation was positioned between the waveguide flanges [24, 25]. The scalar network analyzer records the absolute values (magnitudes) of the microwave scattering parameters (*S*-parameters) in a logarithmic scale. These parameters describe the interaction of an incident electromagnetic wave with the sample and are defined as follows:

$$\begin{aligned} S_{21} &= 10\lg\left(\frac{P_T}{P_I}\right) = 10\lg\left(\frac{E_T^2}{E_I^2}\right) \\ S_{11} &= 10\lg\left(\frac{P_R}{P_I}\right) = 10\lg\left(\frac{E_R^2}{E_I^2}\right) \end{aligned}, \quad (1)$$

where P_I is the power of the incident electromagnetic wave, P_R is the reflected power, and P_T is the power transmitted through the sample (see Fig. 1). Correspondingly, E_I, E_T, and E_R denote the electric field amplitudes of the incident, reflected, and transmitted waves, respectively. The physical meaning of these quantities is straightforward: the parameter S_{11} characterizes the fraction of electromagnetic energy reflected from the sample surface, whereas S_{21} represents the fraction of energy transmitted through the material. Based on the measured *S*-parameters, the electromagnetic wave absorption coefficient *A* (in relative units) can be evaluated using the power balance relation:

$$A = 1 - 10^{\left(\frac{S_{11}}{10}\right)} - 10^{\left(\frac{S_{21}}{10}\right)} \quad (2)$$

During the measurements, the composite specimens were tightly sandwiched between the flanges of the rectangular waveguide, such that the sample plane was oriented perpendicular to the propagation direction of the dominant H_{10} waveguide mode. The lateral dimensions of the samples were sufficiently large to completely fill the waveguide cross-section, thereby preventing electromagnetic leakage around the specimen and ensuring reliable determination of the reflection and transmission characteristics (Fig. 1).

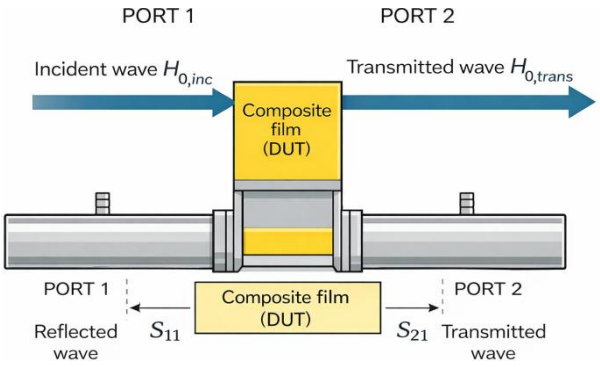

Fig. 1 – Experimental setup for X-band microwave spectroscopy measurements using a rectangular waveguide. The composite film (DUT) is placed perpendicular to the propagation direction of the dominant H_{10} mode. Incident, reflected, and transmitted electromagnetic waves and the corresponding scattering parameters S_{11} and S_{21} are schematically illustrated

3. RESULTS AND DISCUSSION

3.1 SEM EDX

The SEM micrograph of the YIG powder (Fig. 2a) shows a microcrystalline morphology composed of irregularly shaped particles forming loose particle assemblies. The individual YIG particles exhibit characteristic lateral dimensions in the range of approximately 100–300 nm. In addition, larger particle assemblies with sizes of about 1–3 μm are observed, arising from the spatial association of primary particles rather than from dense agglomeration. Based on visual analysis of several representative areas, the average size of the primary YIG particles is estimated to be ~ 180–220 nm, while the typical size of particle assemblies lies around 1.5–2 μm. The particles display a non-spherical morphology with rough, faceted surfaces, which is characteristic of ferrite materials synthesized by solid-state or solution-assisted routes. The absence of compact agglomerates and the presence of loosely connected particle assemblies suggest that YIG can be effectively dispersed within the polymer matrix. The rough particle surface and irregular geometry are expected to promote interfacial contact with the PVC phase, enhancing interfacial polarization effects that contribute to dielectric and microwave losses in PVC/YIG-based composite films. Overall, the SEM observations confirm that YIG consists of microcrystalline particles in the nano–submicron size range, providing a suitable morphological basis for its functional role in electromagnetic shielding and absorption applications.

The SEM micrograph of AC (Fig. 2b) reveals a highly porous, sponge-like morphology characterized by an interconnected network of open and closed pores. The carbon matrix forms irregular, continuous frameworks with thin walls and rounded pore openings, typical of activated carbons obtained via chemical or physical activation. The pore diameters observed on the surface predominantly fall within the range of approximately 0.5–3 μm, while smaller submicron pores (< 500 nm) are also

present but are less clearly resolved at the applied magnification. The solid carbon walls separating adjacent pores typically exhibit thicknesses of about 200–600 nm, with local variations depending on pore geometry. On a larger scale, the AC material consists of micron-sized carbon fragments with characteristic lateral dimensions of approximately 5–20 μm, as estimated from multiple representative regions. These fragments are composed of the aforementioned porous carbon framework rather than discrete particles. The absence of dense particle packing and the dominance of an open porous architecture indicate a large accessible surface area, which is beneficial for interfacial polarization and multiple internal reflections of electromagnetic waves. Such a morphology is expected to favor microwave attenuation through enhanced dielectric losses and scattering effects when AC is incorporated into the PVC/YIG composite matrix. Overall, SEM analysis confirms that activated carbon exhibits a hierarchically porous structure spanning the submicron to micrometer scale, providing a distinct morphological contrast to YIG and carbon nanofillers and explaining its specific contribution to the electromagnetic response of the composite films.

The SEM micrograph of CNPs (Fig. 2c) reveals a morphology composed of quasi-spherical to slightly irregular nanosized carbon particles with relatively smooth surfaces and moderate size dispersion. The particles exhibit clear individual contours and are densely packed, forming a continuous particulate carbon framework. Based on direct measurements from the SEM image, the particle diameters are mainly distributed within the range of approximately 80–250 nm, with the majority of particles falling between 120 and 180 nm. The estimated average particle size is ~150 nm. Occasional larger particles reaching ~ 300 nm are observed, likely originating from partial coalescence during synthesis rather than secondary aggregation. Importantly, the particles retain their individual identity and are in close contact, forming interparticle junctions rather than extended agglomerated clusters. This morphology favors efficient interfacial polarization and charge accumulation at particle–particle and particle–matrix boundaries when embedded in the polymer composite. Compared to AC, CNPs exhibit a significantly narrower particle size distribution and a more homogeneous nanoscale morphology, while lacking the one-dimensional connectivity characteristic of MWCNTs. Such a zero-dimensional particulate structure is expected to enhance dielectric loss mechanisms primarily through Maxwell–Wagner interfacial polarization rather than conductive network formation. Overall, the SEM analysis confirms that the CNPs consist of nanosized carbon particles with an average diameter of ~ 150 nm, providing a high density of interfaces that contributes to the enhanced microwave absorption observed for PVC/YIG/CNP composites.

The SEM image of MWCNTs (Fig. 2d) reveals a dense, highly entangled network of one-dimensional carbon nanostructures forming an interconnected conductive framework. The nanotubes exhibit a characteristic filamentous morphology with frequent bending, overlapping, and interweaving, indicative of a percolated nanotube network. Based on measurements from the SEM micrograph, the outer diameters of individual nanotubes are estimated to be in the range of approximately 15–40 nm, with an average diameter of ~ 25–30 nm. The nanotube lengths significantly exceed the field of view, indicating lengths of at least several micrometers, conservatively estimated as 5–15 μm. This results in a high aspect ratio on the order of 10^2–10^3, which is characteristic of MWCNTs synthesized by catalytic methods. The nanotubes form a continuous, interconnected conductive network rather than isolated bundles, with numerous tube–tube junctions and contact points. Such a morphology is highly favorable for charge transport and the formation of conductive pathways at relatively low filler loadings. In addition, the dense network creates a large number of interfacial regions between the nanotubes and the surrounding matrix, which can act as polarization centers under alternating electromagnetic fields. Compared to zero-dimensional carbon nanoparticles and irregular activated carbon particles, the one-dimensional geometry and high aspect ratio of MWCNTs enable the formation of long-range conductive pathways. This structural feature is expected to significantly enhance dielectric loss through conduction loss and interfacial polarization, explaining the pronounced increase in microwave reflection and absorption observed for the PVC/YIG/MWCNT composites. Overall, the SEM analysis confirms that the MWCNTs consist of thin, high-aspect-ratio nanotubes forming a percolated nanoscale network, which plays a key role in governing the electromagnetic response of the corresponding composite films.

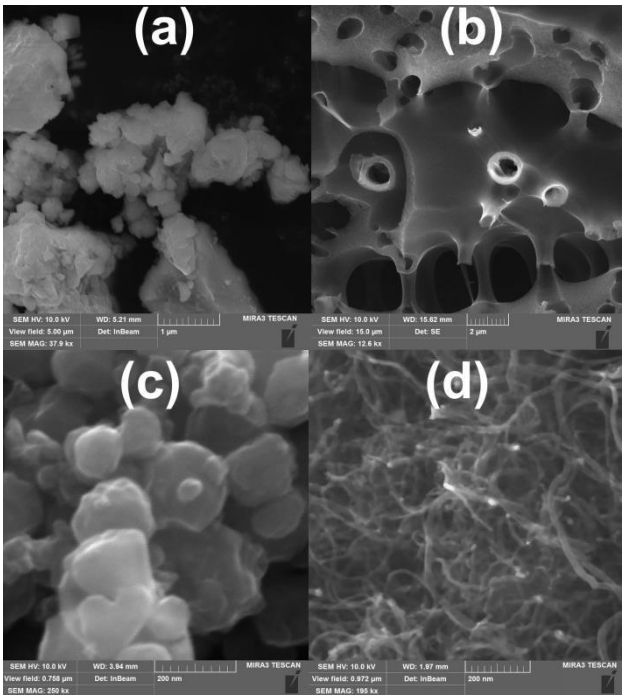

Fig. 2 – (a-d) SEM micrographs of the fillers SEM micrographs of carbon fillers: (a) YIG, (b) AC, (c) CNPs, and (d) MWCNTs.

3.2 EDX

EDX analysis confirms the elemental composition of the investigated fillers and ferrite phase (Fig. 3a-d). For the YIG ferrite, yttrium, iron, and oxygen are clearly detected, and the measured Y/Fe atomic ratio is close to

the nominal stoichiometric value, indicating good compositional uniformity of the ferrite surface (Fig. 3a). Table 1 shows that AC exhibits a dominant carbon content of 92.54 at %, accompanied by 7.46 at % oxygen (Fig. 3b), which can be attributed to surface oxygen-containing functional groups formed during activation. CNPs consist exclusively of carbon within the detection limits of EDX (Fig. 3c), indicating a high degree of purity and the absence of detectable heteroatoms. Acid-treated MWCNTs show a high carbon content of 98.13 at % with a minor oxygen contribution (1.23 at %), reflecting partial surface oxidation after acid treatment. Trace amounts of aluminum (0.33 at %) and iron (0.31 at %) are also detected in MWCNTs, originating from residual catalyst impurities (Fig. 3d).

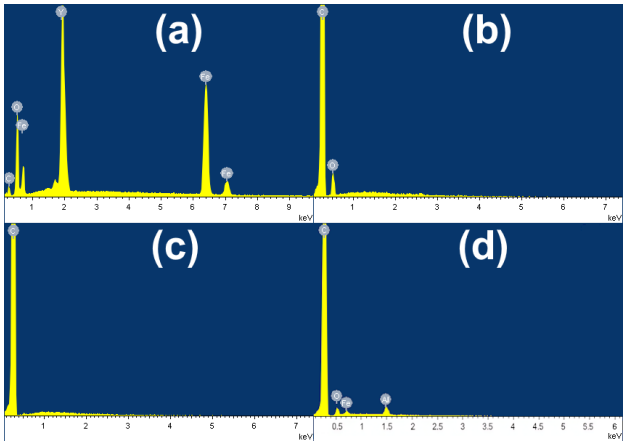

Fig. 3 – (a–d) EDX spectra of (a) YIG ferrite, (b) AC, (c) CNPs, and (d) MWCNTs). The spectra confirm the expected elemental composition of each material.

Table 1 – Description of the elemental composition of carbon fillers determined by SEM-EDX analysis

Filler	Element (at %)	
	C	O
AC	92.54	7.46
CNPs	100	0
[a]MWCNTs	98.13	1.23

[a]Note: MWCNTs contain 0.33 at % Al and 0.31 at % Fe

3.3 Thermogravimetric Analysis

Figure 4 presents the results of thermogravimetric analysis of AC, CNPs, and MWCNTs carried out in an argon atmosphere within the temperature range of 30–800 °C. The studied materials are unmodified and contain only oxygen-containing surface functional groups. Within the temperature interval of 30–800 °C, the vast majority of these functional groups decompose, which makes it possible to obtain information on the surface layer structure and the chemical properties of the carbon materials [21, 22]. The obtained TG–DTG curves indicate a multistage decomposition process of the surface layer of the investigated carbon materials. Since the surface of carbon materials is heterogeneous and contains various structural elements and defects, the temperature intervals of decomposition may differ slightly depending on the nature of the carbon material. An additional influence on the temperature intervals is exerted by the porous structure and diffusion limitations associated with the transport of gaseous decomposition products within small (elongated) pores.

Despite the substantial differences in the nature of the investigated fillers, the overall weight loss is small and amounts to 3–5 %, see Table 2.

Table 2 – Results of DTA of carbon fillers

Filler	TG-DTG		
	$\Delta T_1, \Delta T_2, \Delta T_3$ (°C)	$\Delta m_1, \Delta m_2, \Delta m_3$ (%)	Δm_{tot} (%)
AC	30–163, 163–443, 443–800	0.7, 2.3, 1.8	4.8
CNPs	30–189, 189–400, 400–800	1.1, 0.8, 1.5	3.4
MWCNTs	30–200, 200–383, 383–800	~ 0.0, 1.7, 1.8	3.5

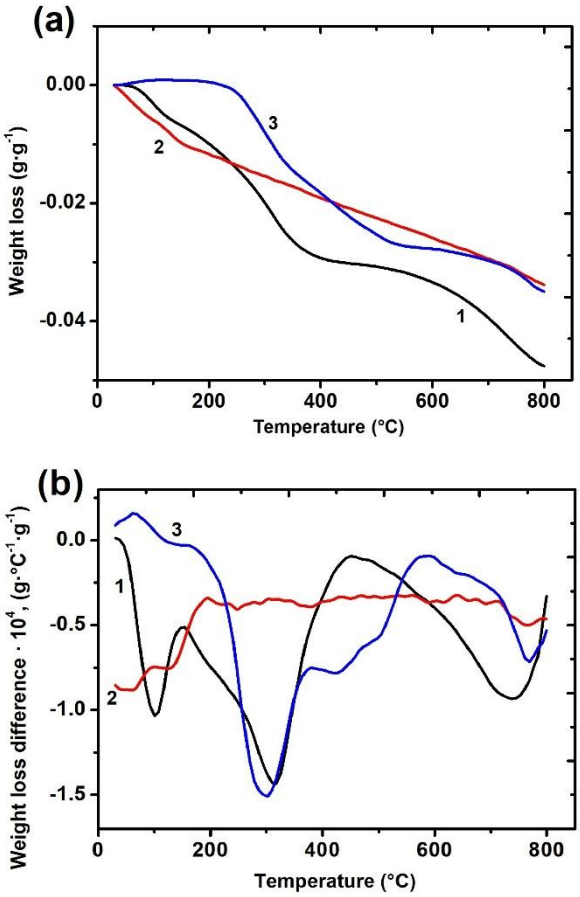

Fig. 4 – TGA of AC, CNPs, MWCNTs in Ar atmosphere: Typical TG (a) and DTG (b) thermograms

This result indicates a low concentration of oxygen-containing functional groups and is in good agreement with the results of our previous studies [21-25].

In the temperature interval ΔT_1 = 30–190 °C, desorption of physically adsorbed water occurs. For AC and CNPs, the weight-loss effects in this interval (Δm_1)

amount to 0.7% and 1.1%, respectively. The most probable adsorption sites for water are micropores and oxygen-containing surface functional groups. For MWCNTs, the corresponding effect is close to zero, which is attributed to the hydrophobic nature of this sample and the low concentration of polar groups. In the temperature interval ΔT_2 = 190–450 °C, decomposition of carboxyl groups as well as the least thermally stable anhydride and lactone groups takes place. For AC and MWCNTs, pronounced weight-loss effects (Δm_2) are observed in this interval, with peak temperatures $T_{2,\,max}$ at 316 and 299 °C, respectively. The estimated concentration of carboxyl groups on the surface of AC and MWCNTs is 0.52 and 0.39 mmol·g^{-1}, respectively. For the CNP sample, the DTG curve does not exhibit distinct extrema, indicating a heterogeneous surface and the presence of functional groups with different decomposition energies. Decomposition of the most thermally stable anhydride, lactone, phenolic, and quinone groups occurs in the temperature interval ΔT_3 = 450–800 °C. For AC, the content of anhydride and lactone groups decomposing in the temperature range of 450–600 °C is relatively low. In contrast, approximately 0.6 mmol·g^{-1} of phenolic groups are present on the AC surface, exhibiting a maximum decomposition rate at $T_{3,\,max}$ = 739 °C. The MWCNT surface contains all types of thermally stable functional groups, and their total amount can be estimated to be 0.50–0.64 mmol·g^{-1}.

Thus, despite significant differences in synthesis methods and structural organization, the investigated carbon materials exhibit a similar surface functional coverage. Various oxygen-containing functional groups are present on the surfaces of AC, CNPs, and MWCNTs, with carboxyl and phenolic groups predominating. At the same time, the studied carbon materials are characterized by a low overall concentration of oxygen-containing groups, which allows them to be classified as non-oxidized carbon materials.

3.4 Optic studies of PVC/YIG/Carbon Composite Films

The optical micro-photographs in Fig. 5 illustrate the surface appearance of PVC/YIG-based composite films and highlight the influence of different carbon fillers on surface texture and optical uniformity. The neat PVC/YIG film (Fig. 5a) exhibits a relatively smooth and homogeneous surface with moderate brightness variations, serving as a reference material without additional carbon fillers. Incorporation of AC (Fig. 5b) results in a distinctly granular and mottled surface morphology accompanied by enhanced light scattering. This behavior is attributed to the relatively large particle size and irregular shape of AC particles, which lead to less uniform dispersion within the polymer matrix. The composite film containing CNPs (Fig. 5c) appears smoother and more uniformly bright, with fewer surface irregularities. This observation suggests a more homogeneous distribution of nanoscale carbon fillers and improved interfacial compatibility with the PVC/YIG matrix. In contrast, the MWCNTs-filled composite (Fig. 5d) shows a relatively uniform coloration combined with a fine speckled texture. This feature is consistent with the formation of an interconnected nanotube network embedded in the polymer matrix, resulting in a characteristic micro-scale contrast pattern. Overall, the optical observations correlate well with the intrinsic morphology and dispersion state of the respective carbon fillers and are consistent with the SEM results. The differences in visible surface texture provide a qualitative indication of variations in filler–matrix interactions and suggest that filler morphology may influence microwave scattering and absorption behavior in the composite films.

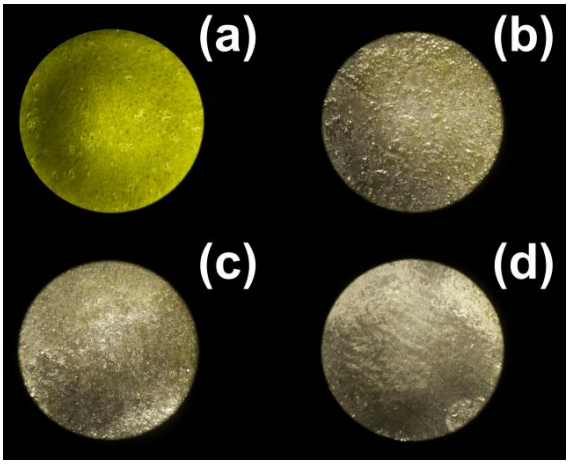

Fig. 5 – Optical microphotographs of prepared composite films arranged as follows: (a) neat PVC/YIG, (b) PVC/YIG/AC, (c) PVC/YIG/CNPs, and (d) PVC/YIG/MWCNTs

3.5 Microwave Properties

An investigation of the microwave properties of the composite films in the X-band (data are presented for three representative frequencies) demonstrates that the nature of the carbon filler has a pronounced effect on the interaction of the composites with electromagnetic radiation. For all studied frequencies, the reflection losses increase significantly compared to pristine PVC (Table 3), with the magnitude of this effect following the trend MWCNTs > CNPs > AC across the entire X-band. Specifically, at 8 GHz, the increase in reflection loss relative to pure PVC amounts to 5.4, 8.6, and 14.2 dB for the AC-, CNP-, and MWCNT-filled composites, respectively. At 10 GHz, the corresponding values are 4.5, 8.9, and 13.5 dB, while at 12 GHz they reach 4.7, 7.6, and approximately 12 dB, respectively.

Table 3 – The reflection losses (RL) evaluated at three selected frequencies

Sample	RL, dB/%		
	8 GHz	10 GHz	12 GHz
PVC	–22.2/0.6	–22.1/0.6	–21.2/0.8
PVC/YIG/AC	–16.8/2.1	–17.6/1.7	–16.5/2.2
PVC/YIG/CNPs	–13.7/4.3	–13.2/4.8	–13.7/4.3
PVC/YIG/MWCNTs	–8.0/16	–8.6/14	–9.3/12

The lowest reflection losses are observed for the PVC/YIG/AC composite, whereas the highest values are recorded for the PVC/YIG/MWCNTs system, indicating that the AC-filled film exhibits the weakest electromagnetic reflection in this frequency range, while the MWCNT-filled film reflects electromagnetic radiation

most strongly. When expressed as reflection percentages, the average reflected power for the AC-, CNP-, and MWCNT-based composites is approximately 2%, 4.5%, and ~14%, respectively (Table 3). Consequently, the reflection level of the MWCNT-filled film is about 12% higher than that of the AC-based composite.

The transmission of electromagnetic waves for all studied samples decreases slightly compared to pristine PVC, with the magnitude of attenuation following the trend MWCNTs < CNPs < AC across the entire X-band (Table 4).

Table 4 – The transmission losses (TL) evaluated at three selected frequencies

Sample	TL, dB/%		
	8 GHz	10 GHz	12 GHz
PVC	–0.34/92	– 0.22/95	– 0.10/98
PVC/YIG/AC	–0.35/92	– 0.28/94	– 0.32/93
PVC/YIG/CNPs	–1.59/69	– 1.38/73	– 1.47/71
PVC/YIG/MWCNTs	–2.16/61	– 2.22/60	– 2.42/57

At 8 GHz, the reduction in transmission relative to pure PVC amounts to 0, 1.2, and 1.8 dB for the MWCNT-, CNP-, and AC-filled composites, respectively. At 10 GHz, the corresponding values are 0.05, 1.16, and approximately 2 dB, while at 12 GHz they reach 0.22, 1.4, and 2.3 dB, respectively. The smallest decrease in transmission is observed for the PVC/YIG/AC composite, whereas the largest attenuation occurs for the PVC/YIG/MWCNT system. This indicates that the AC-filled film exhibits the weakest suppression of electromagnetic wave transmission in the studied frequency range, while the MWCNT-filled composite shows the strongest reduction. When expressed in percentage terms, the average transmission values for the AC-, CNP-, and MWCNT-based composites amount to approximately 93%, 71%, and 59%, respectively (Table 2). Consequently, the transmission level of the MWCNT-filled film is approximately 33% lower than that of the AC-based composite (Table 4).

Table 5 – The absorption (*A*) evaluated at three selected frequencies

Sample	*A*, %		
	8 GHz	10 GHz	12 GHz
PVC	6.97	4.39	1.57
PVC/YIG/AC	5.62	4.41	4.86
PVC/YIG/CNPs	26.27	22.44	24.35
PVC/YIG/MWCNTs	23.30	26.13	30.87

The absorption of electromagnetic waves increases markedly for all studied frequencies compared to pristine PVC (Table 5), with the magnitude of absorption following the trend MWCNTs > CNPs > AC across the entire X-band. At 8 GHz, the absorption increases from 5.6% for the AC-filled composite to 26.3% for the CNP-containing film. At 10 GHz, the absorption rises from 4.4% (AC) to 26.1% (MWCNTs), while at 12 GHz it increases from 4.9% (AC) to approximately 31% (MWCNTs). Compared to pure PVC, the smallest change in absorption is observed for the PVC/YIG/AC composite (4.3% *vs* 4.9%, respectively), whereas the largest enhancement occurs for the PVC/YIG/MWCNT system (4.3% *vs* 26.8%, respectively). These results indicate that the composite film containing activated carbon exhibits the weakest electromagnetic wave absorption in the studied frequency range, while the MWCNT-filled composite demonstrates the strongest absorption. Thus, among the three investigated carbon fillers, MWCNTs provide the most effective absorption of electromagnetic radiation in the X-band. Considering the relatively small film thickness (0.25 mm), the achieved absorption levels can be regarded as notably high, underscoring the efficiency of MWCNT-based composites for microwave attenuation applications.

4. DISCUSSION

The obtained results indicate that the microwave response of PVC/YIG/carbon composite films in the X-band is governed primarily by the morphology, electrical conductivity, and dispersion state of the carbon fillers rather than by their mere presence. The comparative analysis of reflection, transmission, and absorption reveals distinct interaction mechanisms for composites containing AC, CNPs, and MWCNTs. The observed increase in reflection losses for all composites relative to pristine PVC can be attributed to enhanced effective permittivity and electrical conductivity upon incorporation of carbon fillers. The highest reflection losses are found for MWCNT-filled composites, which is consistent with the suggested formation of well-developed percolation networks arising from the high aspect ratio and intrinsic conductivity of nanotubes. These conductive pathways presumably promote strong impedance mismatch with free space, leading to increased electromagnetic reflection. In contrast, AC-filled composites exhibit the lowest reflection losses due to their lower electrical connectivity and fragmented conductive structure. Microwave transmission through the composite films decreases only moderately compared to PVC; however, a clear dependence on filler type is observed. The smallest attenuation occurs for AC-based composites, whereas the strongest suppression of transmission is characteristic of MWCNT-containing films. This behavior reflects the increasing density of conductive pathways and internal scattering centers, which enhance attenuation within the material. The most significant differences among the composites are observed in their absorption behavior. Absorption increases markedly for all carbon-filled systems compared to PVC, following the trend AC < CNPs < MWCNTs across the entire X-band. The superior absorption performance of MWCNT-based composites can be attributed to a combination of conductive losses within the nanotube network, interfacial (Maxwell–Wagner–Sillars) polarization at numerous polymer–filler interfaces, and multiple internal scattering within the heterogeneous nanostructure. Composites containing CNPs show intermediate absorption, reflecting their large interfacial area but less effective three-dimensional conductive connectivity. Despite its high surface area, activated carbon provides the weakest absorption enhancement due to its discontinuous morphology and limited electrical transport. Importantly, the relatively high absorption achieved at a small film thickness of

0.25 mm highlights the efficiency of MWCNTs as functional fillers for thin and lightweight microwave-absorbing materials. Overall, the balance between controlled reflection, moderate transmission, and high absorption makes PVC/YIG/MWCNT composites particularly promising for electromagnetic interference mitigation and microwave attenuation applications where absorption-dominated mechanisms are preferred.

5. CONCLUSIONS

Flexible composite thin films based on PVC and filled with YIG and carbon materials of different morphology were successfully fabricated and investigated. The films were produced by thermal hot pressing using ball-milled YIG powders and DBP as a plasticizer, while the carbon fillers were mechanically ground prior to incorporation to ensure uniform dispersion within the polymer matrix. Microwave measurements performed in the X-band (8–12 GHz) for composites containing 20 wt.% YIG and 10 wt.% carbon filler revealed a strong dependence of electromagnetic properties on the nature of the carbon component. Compared with neat PVC, electromagnetic wave reflection increased across the entire frequency range, following the trend MWCNTs > CNPs > AC, while transmission decreased in the opposite order (AC > CNPs > MWCNTs). Correspondingly, microwave absorption increased from approximately 5% for AC-filled composites to about 24% for CNP-filled and ~27% for MWCNT-filled films, demonstrating that carbon nanotubes provide the most effective absorption among the investigated fillers. Overall, the results demonstrate that carbon filler morphology plays a decisive role in tuning the microwave response of PVC/YIG/carbon composites. The combination of high ferrite content with conductive carbon fillers, particularly MWCNTs, enables enhanced microwave absorption in thin and flexible films, making these materials promising candidates for lightweight radio-absorbing and electromagnetic interference shielding coatings. Future work will focus on optimizing filler ratios and film thickness, as well as extending the investigation to broader frequency ranges to further enhance absorption performance.

ACKNOWLEDGMENTS

M. I. P. is in debt to partial support by the Ministry of Education and Science of Ukraine: Grant for the perspective development of the scientific direction: "Mathematical Sciences and Natural Sciences" at the Taras Shevchenko National University of Kyiv. L. M. G. and V. E. D. in debt to the Presidium of the National Academy of Science of Ukraine for the partial support of the work. The authors acknowledge the National Research Foundation of Ukraine (NRFU) and the “Excellent Science in Ukraine” program (Grant No. 2023.03/0193) for supporting the morphological investigations.

REFERENCES

1. S. Cucurachi, et al., *Environ. Int.* **51**, 116 (2013) https://doi.org/10.1016/j.envint.2012.10.009.
2. S. Singh, N. Kapoor, *Adv. Biol.* **2014**, 198609 (2014) https://doi.org/10.1155/2014/198609.
3. M.S. Markov, *Electromagnetic Fields in Biology and Medicine*, 1st ed. (CRC Press, Boca Raton, USA, 2015). https://doi.org/10.1201/b18148.
4. I. Belyaev, *in Mobile Communications and Public Health, edited by M. Markov* (CRC Press, Boca Raton, USA, 2019), pp. 65–101.
5. M. Jaroszewski, S. Thomas, A.V. Rane, *eds. Advanced Materials for Electromagnetic Shielding: Fundamentals Properties, and Applications* (Wiley, New York, USA, 2018) https://doi.org/10.1002/9781119128625.
6. Q. Nguyen, C. Choi, *Heliyon* **10** No 10, e31118 (2024) https://doi.org/10.1016/j.heliyon.2024.e31118.
7. J. Li, et al., *Carbon* **224**, 119058 (2024) https://doi.org/10.1016/j.carbon.2024.119058.
8. F. Zhang, et al., *Compos. B: Eng.* **283**, 111646 (2024) https://doi.org/10.1016/j.compositesb.2024.111646.
9. J. Liu, et al., *Chem. Eng. J.*, **496**, 154013, (2024) https://doi.org/10.1016/j.cej.2024.154013.
10. O.P. Grigoryeva, et al., *IEEE 15th International Conference Nanomaterials: Applications & Properties* (NAP), Bratislava, Slovakia, 2025, pp. MT04-1-MT04-6. https://doi.org/10.1109/NAP68437.2025.11216252.
11. B. Wen, et al., *J. Colloid. Interface Sci.* **626**, 759 (2022) https://doi.org/10.1016/j.jcis.2022.06.141.
12. X. Zhang, et al., *Carbon* **177**, 216 (2021) https://doi.org/10.1016/j.carbon.2021.02.085.
13. Y. Liu, et al., *J. Mater. Sci. Technol.* **103**, 157 (2022) https://doi.org/10.1016/j.jmst.2021.06.034.
14. T.T. Si, et al., *J. Mater. Sci. Mater. Electron.* **34**, 1035 (2023) https://doi.org/10.1007/s10854-023-10468-w.
15. S. Sumanta, K. Rajesh, S.H. Sung, *New Carbon Mater.* **40** No 2, 293 (2025) https://doi.org/10.1016/S1872-5805(25)60965-6.
16. Z. Cui, et al., *Carbon* **230**, 119627 (2024) https://doi.org/10.1016/j.carbon.2024.119627.
17. Y. Lin, et al., *J. Mater. Sci: Mater. Electron.* **27** No 8, 8177 (2016) https://doi.org/10.1007/s10854-016-4821-x.
18. Y. Lin, et al., *Mater. Lett.* **93**, 230 (2013) https://doi.org/10.1016/j.matlet.2012.11.087.
19. H.B. Yang, et al., *Mater. Lett.* **145**, 19 (2015) https://doi.org/10.1016/j.matlet.2015.01.080.
20. J. Jiang, L.H. Ai, L.C. Li, *J. Phys. Chem. B* **113** No 5, 1376 (2009) https://doi.org/10.1021/jp808270n.
21. L.M. Grishchenko, et al., *IEEE 7th International Conference Nanomaterials: Application & Properties* (NAP), Odessa, Ukraine, 2017, pp. 01PCSI19-1-01PCSI19-6 https://doi.org/10.1109/NAP.2017.8190155.
22. L.M. Grishchenko, et al., *Mol. Cryst. Liq. Cryst.* **673** No 1, 1 (2018) https://doi.org/10.1080/15421406.2019.1578488.
23. A.N. Zaderko, et al., *Appl Nanosci* **12**, 361 (2022) https://doi.org/10.1007/s13204-020-01651-0.
24. L.M. Grishchenko, et al., *IEEE 42th International Conference on Electronics and Nanotechnology* (ELNANO-2024), art. No 81, 161 (Kyiv: Igor Sikorsky Kyiv Polytechnic Institute: 2024) https://doi.org/10.1109/ELNANO63394.2024.10756899.
25. L.M. Grishchenko, et al., *Mol. Cryst. Liq. Cryst.* **751** No 1, 1 https://doi.org/10.1080/15421406.2022.2073045.

Мікрохвильова поведінка композитних плівок ПВХ/ЗІГ/Вуглецевий матеріал у Х-діапазоні

Л.М. Гріщенко[1,2], Д.О. Житник[3], В.Ю. Малишев[3], В.Є. Діюк[2,3], Т.О. Плутенко[4], М.О. Попов[3], Г.Л. Чумак[3], І.П. Матушко[3], Ю.В. Носков[5], В.В. Кириченко[3], М.В. Макарець[3], В.В. Лісняк[1,6].

[1] *Інститут хімії поверхні імені О.О. Чуйка, Національна академія наук України, 03164 Київ, Україна*
[2] *Інститут технічної теплофізики, Національна академія наук України, 03057 Київ, Україна*
[3] *Київський національний університет імені Тараса Шевченка, 01601 Київ, Україна*
[4] *Інститут загальної та неорганічної хімії імені В.І. Вернадського, Національна академія наук України, 03142 Київ, Україна*
[5] *Інститут біоорганічної хімії та нафтохімії імені В.П. Кухаря, Національна академія наук України, 02160 Київ, Україна*
[6] *Інститут хімії високомолекулярних сполук, Національна академія наук України, 02155 Київ, Україна*

У даній роботі представлено виготовлення та дослідження мікрохвильових властивостей гнучких композиційних плівок на основі полівінілхлориду (ПВХ), що містять залізо-ітрієвий гранат (ЗІГ) та вуглецеві наповнювачі різної морфології, а саме багатостінні вуглецеві нанотрубки (ВНТ), вуглецеві наночастинки (ВНЧ) і активоване вугілля (АВ). Композиційні плівки товщиною близько 0,25 мм отримували методом гарячого пресування при 175 °C та тиску 10 МПа з використанням 20 мас.% ЗІГ, 10 мас.% вуглецевого наповнювача (відносно ПВХ) та дибутилфталату як пластифікатора. Використані наповнювачі було охарактеризовано методами сканувальної електронної мікроскопії (СЕМ) та термогравіметричного аналізу. Згідно даних СЕМ, порошок ЗІГ складається з агломерованих квазі-сферичних кристалітів. ІЧ-спектри композиційних плівок демонстрували характерні смуги поглинання ПВХ та ЗІГ; при введенні наповнювачів спостерігалися незначні зсуви окремих характеристичних смуг полімеру, що вказує на незначну взаємодію між наповнювачами та ПВХ-матрицею. Мікрохвильові вимірювання у Х-діапазоні (8–12 ГГц) показали суттєву залежність коефіцієнтів відбиття, проходження та поглинання від природи вуглецевого наповнювача. Порівняно з чистим ПВХ, поглинання електромагнітних хвиль істотно зростає у ряду ВНТ > ВНЧ > АВ в усьому дослідженому частотному діапазоні. За частоти 8 ГГц поглинання зростає від приблизно 5,6% (АВ) до 26,3% (ВНЧ); за 10 ГГц – від 4,4% (АВ) до 26,1% (ВНТ); за 12 ГГц – від 4,9% (АВ) до 31% (ВНТ). Найменше зростання поглинання спостерігалося для композиту ПВХ/ЗІГ/АВ, тоді як найбільше – для плівок ПВХ/ЗІГ/ВНТ. Отримані результати свідчать про те, що морфологія вуглецевого наповнювача відіграє вирішальну роль у формуванні мікрохвильових поглинальних властивостей композицій ПВХ/ЗІГ/вуглець. Серед досліджених наповнювачів ВНТ забезпечують найефективніше мікрохвильове поглинання у Х-діапазоні, що підкреслює перспективність цих трикомпонентних композицій для використання у легких, гнучких мікрохвильових поглинаючих та екрануючих покриттях, що забезпечить захист від електромагнітного випромінювання.

Ключові слова:. Залізо-ітрієвий гранат, Полівінілхлорид, Композитний матеріал, Вуглецеві матеріали, Електромагнітне екранування, Матеріали, що поглинають мікрохвилі.